

# Case Study on Applications of Structural Fuses in Bridge Bents

Xiaone Wei<sup>1</sup> and Michel Bruneau, F.ASCE<sup>2</sup>

**Abstract:** In seismic design, bridges are typically designed to undergo inelastic deformations during a severe earthquake. In those instances, most of the seismic energy is dissipated through hysteretic behavior of the critical load-resisting components, which results in permanent deformations and damage and could make repairs expensive or, in some cases, impossible. Thus, concentrating earthquake damage in structural fuses inserted in bridge bents is desirable; the performance objective is for the main gravity load-bearing members (the columns, in this case) to be intact after an earthquake, limiting repairs to fuses that can be removed and replaced easily. This paper presents results from case studies that considered the use of buckling-restrained braces (BRBs) as hysteretic energy-dissipation devices inserted in bridge bents to dissipate earthquake energy and improve structural performance by minimizing inelastic demands on the columns. A typical California bridge was used for this purpose. For structural fuse application only in the transverse direction (along the bent), results indicate that BRBs are implementable. Alternative bent configurations were also considered to provide the benefit of structural fuses for seismic excitations in the bridge's longitudinal and transverse directions. Findings are presented along with observations from a comparison of seismic responses between bridges with and those without structural fuses in their bents. DOI: [10.1061/\(ASCE\)BE.1943-5592.0000854](https://doi.org/10.1061/(ASCE)BE.1943-5592.0000854). © 2016 American Society of Civil Engineers.

**Author keywords:** Buckling-restrained braces; Structural fuse; Seismic analysis; California bridges; Columns; Earthquake-resistant design.

## Introduction

Seismic bridge design procedures still rely, to a large degree, on the detailing of bridge columns for ductile response to provide lateral load resistance. Because columns are also part of the gravity load-resisting system, inelastic deformations in columns may compromise the stability of a bridge during an earthquake or result in permanent damage that is beyond repair afterward. For well-detailed ductile RC columns, prevention of the bridge's total collapse can be achieved, but the seismic damage sustained can often require temporary closure of the bridge for days or even weeks to bring it back to service condition. From a postearthquake perspective, accelerated bridge construction (ABC) implies an ability to expedite bridge repairs and, if possible, execute those repairs while keeping the bridge open or, at worst, limiting disturbance by requiring only short-duration closures (typically by accomplishing work at night). Toward that objective, using structural fuses (SFs) is attractive, because they dissipate hysteretic energy in select structural elements separate from the columns in such a way that the columns are left intact and the fuses can be removed and replaced.

In this paper, buckling-restrained braces (BRBs) are investigated as SFs implemented in a typical California bridge (or types of bridges that would be compatible with Caltrans practice). A

corresponding design procedure is proposed; concrete-filled steel tube (CFT) columns were used and BRBs were sized to meet the SF objectives under the governing seismic lateral loads for two proposed bridge bent configurations. First, a two-column bent (considering single-inclined BRB and inverted-V BRB configurations), for which response of the bent under seismic excitation in the transverse direction, was studied with the understanding that this implementation of the fuse strategy would have to be coupled with another system in the longitudinal direction (which could be, e.g., SFs in series with lock-up devices connecting the bridge deck to the abutments). Second, a box-pier configuration was designed to allow for the implementation of SFs to resist earthquake excitations in both longitudinal and transverse directions. Pushover analyses were performed to investigate seismic demands on the columns, and theoretical and actual pushover curves were compared. A seismic and service load demand check on the CFT columns was conducted. Results from nonlinear time-history analyses of all the bridge bents with BRBs, subjected to spectrum-compatible synthetic ground motions, are presented and verified with the bridge bent displacements predicted from the design procedure. The displacement demands of the systems with BRBs were also compared with those corresponding bridge bents without BRBs to quantify the benefit of adding BRBs into the bridge bents. Note that the concept proposed here would be applicable only when no traffic is permitted between the columns tied by the BRBs (unless horizontal and vertical clearances can be ensured). Furthermore, the aesthetics of the proposed concept, which may be a concern to some, is beyond the scope of this paper and best left to individual DOTs and bridge owners to assess.

Although BRBs have never been used in the SF application presented in this case study, BRBs have been used extensively in buildings and are starting to be used more frequently in bridges. Initially developed in Japan in the mid-1980s (then referred to as unbounded braces), BRBs have been implemented in North America since the late 1990s. Although a variety of BRB concepts have been developed

<sup>1</sup>Graduate Research Assistant, Dept. of Civil, Structural, and Environmental Engineering, Univ. at Buffalo, Buffalo, NY 14260 (corresponding author). E-mail: [xiaonewe@buffalo.edu](mailto:xiaonewe@buffalo.edu)

<sup>2</sup>Professor, Dept. of Civil, Structural, and Environmental Engineering, Univ. at Buffalo, Buffalo, NY 14260. E-mail: [bruneau@buffalo.edu](mailto:bruneau@buffalo.edu)

Note. This manuscript was submitted on December 18, 2014; approved on September 14, 2015; published online on February 8, 2016. Discussion period open until July 8, 2016; separate discussions must be submitted for individual papers. This paper is part of the *Journal of Bridge Engineering*, © ASCE, ISSN 1084-0702.

and patented, a BRB generally consists of a central core surrounded by a tube that restrains the core from axial global buckling in compression.

Extensive analytical and experimental research has been conducted using BRBs to reduce the inelastic deformations of the existing building frames (Wada et al. 2000; Aiken et al. 2000; Clark et al. 2000; Lopez et al. 2002). Descriptions of the mechanics of BRBs with fully detailed design examples as BRB frames were presented by López and Sabelli (2004). Applications of BRBs in bridges were recently contemplated and, in a few cases, implemented. Usami et al. (2005) studied the implementation of BRBs for the seismic upgrading of steel arch-truss bridges, such as the long-span Minato Bridge in Japan, which was retrofitted by installing BRBs on the cross frames of the main tower and on the lower lateral bracing near the main tower (Hamada et al. 2007). Also, Kanaji et al. (2005) reported that analyses of the retrofitted bridge proved that BRBs were effective in preventing buckling or yielding of the other main members of the bridge. BRBs were also implemented in the seismic retrofit of a parabolic haunched deck-truss superstructure (the Auburn-Foresthill Road Bridge in northern California) by replacing the horizontal chevron bracing members near the abutment and longitudinal struts with BRBs to control loads in the critical load path system (Reno and Pohl 2010). Other example applications include the Araku-bashi Bridge, a rigid frame bridge with a knee brace in which a new type of T-BRBs with steel mortar planks was used (Oya et al. 2009), and the Owatari Bridge, the first new arch-truss bridge built with BRBs to enhance its seismic performance. Another possible use of BRBs was studied for the Vincent Thomas suspension bridge in California to replace the viscous fluid dampers that are part of the existing seismic mitigation system (Lanning et al. 2011).

Other promising applications of BRBs in bridges include new bridge column configurations, such as the twin-column bridge studied by El-Bahey and Bruneau (2010), and ductile end cross frames in slab-on-girder bridges, such as those studied by Carden et al. (2006) as an implementation of the ductile diaphragm concept developed by Zahrai and Bruneau (1999). Actual implementation of BRBs as a ductile cross-frame concept in a new bridge was shown by Uang et al. (2014). Figures for the other bridge applications of the BRBs mentioned here can be found in Wei and Bruneau (2013) and Uang et al. (2014).

In contrast to these studies and implementations, for the case study presented here, the authors considered the possible implementation of BRBs in the conventional bents of standard highway bridges, as part of a SF concept, which has not been attempted before.

## SF Concept

A SF system can be divided into two parts, namely, the frame that is intended to remain elastic (i.e., the bare bridge bent in this case) and the SF that is the hysteretic energy-dissipating element. In a generic sense, the overall stiffness of the bridge bent,  $K_{tot}$ , is equal to the sum of the lateral stiffness,  $K_s$ , provided by the SF, and the lateral stiffness of the bare bridge bent,  $K_f$ . Correspondingly, a stiffness ratio,  $\alpha$ , is defined as the ratio between  $K_s$  and  $K_f$  such that

$$K_{tot} = K_f + K_s \quad (1)$$

$$\alpha = \frac{K_s}{K_f} \quad (2)$$

The system's displacement ductility capacity,  $\mu_D$ , which is the maximum ductility that the SF can develop before the bent column yields, is defined as

$$\mu_D = \frac{\Delta_{yf}}{\Delta_{ys}} \quad (3)$$

where  $\Delta_{ys}$  = displacement reached by the bridge bent when the SF yields; and  $\Delta_{yf}$  = yield displacement of the corresponding bare bridge bent.

The most efficient use of SF is achieved when the difference between bare bent and fuse yield displacement is maximized. Other useful nondimensional parameters related to the strength of the system include the seismic demand of the total system,  $V_e$ , if the system behaved elastically up to the corresponding expected displacement,  $\delta_e$ ; the yield strength of the bare bent,  $V_{yf}$ , which is the force resisted by the bare bent when the yield displacement of the column is reached; and the yield strength of the SF,  $V_{ys}$ , which is the force resisted by the fuse after the fuse yields. The maximum displacement ductility that the bridge bent needs to withstand is given by the ductility ratio calculated at the system displacement reached for the maximum credible earthquake (expected displacement),  $\delta_e$ . When the expected displacement  $\delta_e$  is in the constant-velocity region of the spectrum

$$\delta_e = \frac{V_e}{K_{tot}} \quad (4)$$

For the SF system to be effective, the expected displacement  $\delta_e$  should be larger than the yield displacement  $\Delta_{ys}$  that the bent reaches when the SF yields but smaller than the yield displacement  $\Delta_{yf}$  that corresponds to yielding of the bent columns. Among all the parameters already defined, the ductility factor  $\mu_D$  and the stiffness ratio  $\alpha$  can be thought of as those that govern the design of the SFs for the system. The pushover force-displacement curves are shown in Fig. 1 for the bare bent, the SF, and the total SF system, with the displacement and force notation already defined. More information on this SF concept is available elsewhere [e.g., Vargas and Bruneau (2006) and El-Bahey and Bruneau (2010)].

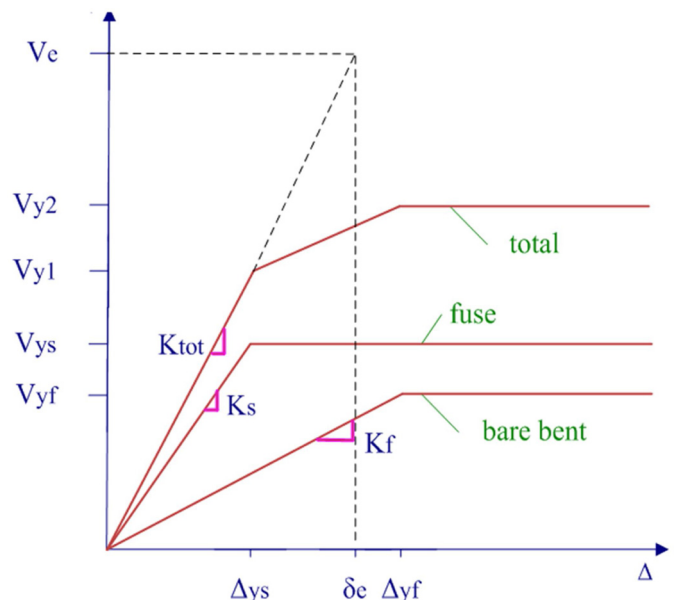
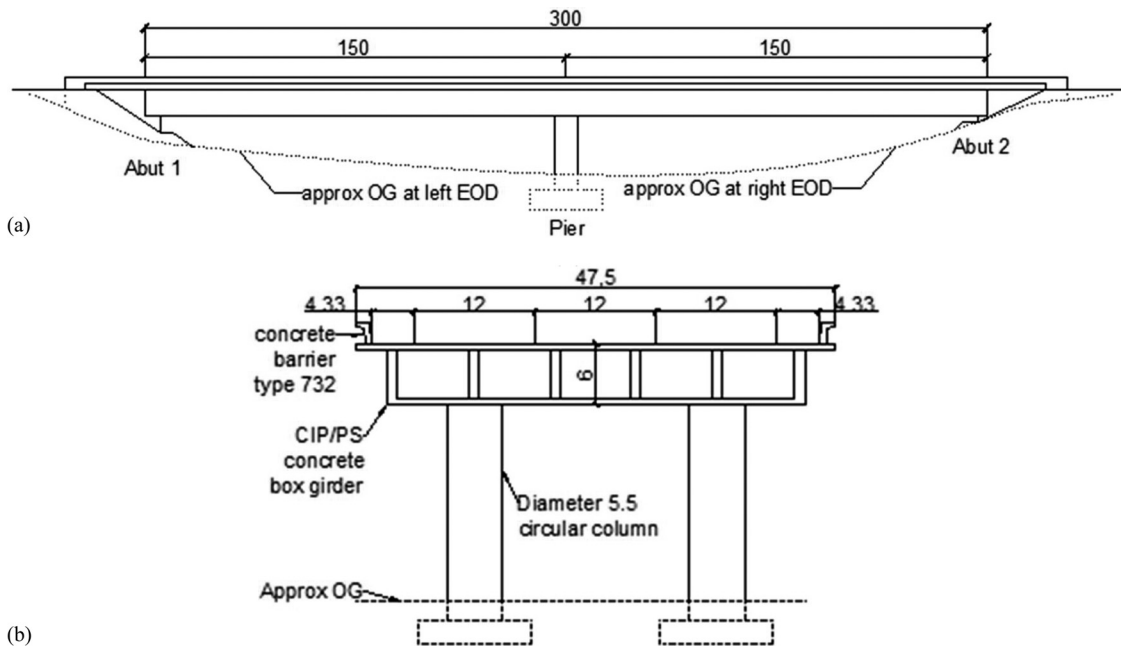


Fig. 1. General pushover curve for the bridge bent system with structural fuses



**Fig. 2.** Caltrans OSB1: (a) elevation; (b) bridge bent at the center of the bridge span (Note: Unit = ft; OG = original ground; EOD = edge of deck; CIP = cast in place; PS = prestressed)

### Proposed Design Procedures

This case study focuses on the Caltrans generic bridge Ordinary Standard Bridge 1 (OSB1), for which drawings were provided by Caltrans for this purpose. This two-span continuous bridge has a total abutment-to-abutment length of 91.4 m (300 ft) and is supported on an integral two-column bent at midspan (as shown in Fig. 2). Although the use of RC columns was considered in the early phases of the study, the final designs were made with CFT columns, because it was found to facilitate the design of the SF system and connection of BRBs to the columns.

The flowchart in Fig. 3 summarizes the design procedure of the proposed bridge bent with SFs, recognizing that the process was iterative. Following that flowchart, the design procedure can be broken down in the following steps.

#### Step 1: Calculations of the Bent Target Displacement and Bare Bent Stiffness

The maximum displacement permissible with the SF concept is set equal to the yield displacement of the column (also called the *expected displacement* in subsequent steps), which can be calculated when the stiffness of the bare bent is known. For preliminary design, to size a column's diameter, the gravity dead load of the bridge's superstructure tributary to the column bent was assumed to be distributed equally to each column of the center bridge bent, and dead-load demand was taken to be approximately 5% of the overall axial strength of each CFT column. Note that CFT columns have no reinforcement in the concrete infill and that their properties and strengths (in particular, their cross-section axial compressive and tensile strength, flexural strength, and yielding curvature) were obtained through fiber analysis using the program Section Designer in SAP2000 14. The buckling compressive strength of the column was checked using equations from AISC (2010) for composite members. The yield displacement,  $\Delta_y$ , and the effective stiffness of the CFT column,  $K_{col}$ , were calculated as

$$\Delta_y = 2\varphi_y \frac{(h/2)^2}{3} \quad (5)$$

$$K_{col} = \frac{2M_y}{h\Delta_y} \quad (6)$$

where  $\varphi_y$  = yield curvature of the CFT section;  $h$  = height of the CFT column; and  $M_y$  = yield strength of the CFT column. Note that OSB1 has an integral bent with columns fixed at the top of the cap beam. For a nonintegral bent, the bare bent stiffness would be smaller, and the stiffness of the BRB needed to achieve the SF design objective would be different, but the design methodology would remain the same.

#### Step 2: Calculation of Required Fuse Stiffness

The required fuse stiffness is selected to be the minimum value required to prevent column yielding. For this purpose, the expected

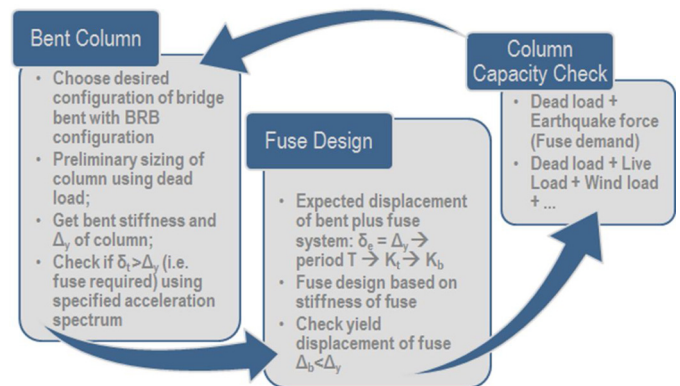


**Fig. 3.** Design flowchart of a bridge bent with BRBs

displacement of the bridge bent with BRBs,  $\delta_e$ , was calculated on the basis of the assumption of equal elastic and inelastic displacements for a given period commonly used in earthquake-resistant design. As mentioned in Step 1, it was set to be equal to the yield displacement of the column,  $\Delta_y$ . The provided acceleration spectrum gives a relationship between the maximum acceleration,  $S$ , and period,  $T$ , by Eq. (7). The total stiffness of the bridge bent with BRBs was derived for the given superstructure weight,  $W_{\text{super}}$ , in Eq. (8), assuming that no lateral resistance was provided by the abutments. The self-weight of the columns was ignored because it is typically small compared with that of the superstructure. The expected displacement of the bare bridge bent,  $\delta_t$ , was calculated using Eq. (9) and verified to be larger than the columns' yield displacement  $\Delta_y$ , which makes the addition of BRBs worthwhile in reducing the displacement demand.

$$\delta_e = S_a T_s^2 \frac{g}{4\pi^2} = \Delta_y \quad (7)$$

$$K_t = \frac{W_{\text{super}} 4\pi^2}{386 T_s^2} \quad (8)$$

$$\delta_t = S_b T_1^2 \frac{g}{4\pi^2} \quad (9)$$

where  $S_a$  and  $S_b$  = accelerations from the target spectrum and corresponding to the period of the bridge bent with BRBs,  $T_s$ , and period of the bare bridge bent,  $T_1$ , respectively, which is equal to

$$\sqrt{\frac{W_{\text{super}} 4\pi^2}{386 K_c}}$$

and,  $K_t$  and  $K_c$ , = stiffness of the total bridge bent with BRBs and of the bare bridge bent, respectively.

### Step 3: BRB Design

The BRB was designed to reach a strain limit of 1.5% in the yield core when the columns reach their yield displacement,  $\Delta_y$ . Note that strains up to 3% can typically be developed in BRBs and that such a limit could have been used instead, resulting in smaller BRBs. Fig. 4(a) schematically illustrates the composition of a BRB and identifies three specific zones: the yield core at the center of the BRB restrained from buckling, the buckling-restrained transition segments, and the non-yielding unrestrained end zones at the two ends.

For the two general bridge configurations, namely, two-column bent with BRBs and box-pier bent with BRBs, the area and length ratios of the required BRBs were designed differently.

#### Two-Column Bent with BRBs

The behavior of this system depends on the length ratio of the yield core length to the entire BRB length,  $c_b$  [given by Eq. (10)], and the angle of the BRB from the horizontal,  $\theta$ , which differs for the single-inclined and inverted-V BRB cases.

$$c_b = \frac{\Delta_y}{\varepsilon_{\text{bm}} L_{\text{brb}}} \quad (10)$$

where  $\varepsilon_{\text{bm}}$  = strain limit of the BRB's yielding core; and  $L_{\text{brb}}$  = length of the BRB. Figs. 4(b and c) show the two-column bridge

bent BRBs. The foundation of the bent column is shown in Fig. 4(d) with the eccentricity between the point at which the brace and the column's actual workline meet. The eccentricity causes a larger reaction force at the bottom of the column, whereas the forces from the BRB would go to the foundation if the eccentricity does not exist.

The displacement of the bent corresponding to the yielding of BRB,  $\Delta_b$ , as a minimum requirement for the SF concept to work, must be smaller than the expected displacement of the bridge bent,  $\delta_e$ , which is expressed by Eq. (11)

$$\Delta_b = \frac{f_{yb} c_b L_{\text{brb}}}{E_s \cos \theta} < \delta_e \quad (11)$$

where  $f_{yb}$  = yield strength of the steel used in the BRB's core, assumed in this case study to be A36 with an expected yield strength of  $2.89 \times 10^5$  kPa (42 ksi). On the basis of the required BRB stiffness obtained from Step 2, the stiffness of each BRB is  $K_b$ , which is equal to  $K_t - K_c$  in the single-inclined BRB case and  $(K_t - K_c)/2$  in the inverted-V BRB case. Therefore, the cross-sectional area of each BRB,  $A_{\text{brb}}$ , is

$$A_{\text{brb}} = \Delta_b \frac{K_b}{f_{yb} \cos \theta} \quad (12)$$

#### Box-Pier Bent with BRBs

The box-pier bridge configuration, together with a close-up view of the midspan bridge bent, is shown in Fig. 5. The typical geometry of a box-pier bent with BRBs is shown in Fig. 6. The number of BRBs between the closely spaced CFT columns in the composite box pier can generically be taken as  $n$ . For example, for the bridge bent in Fig. 6,  $n = 4$ . In this case, the length ratio of BRB,  $c_b$ , is

$$c_b = \frac{\Delta_y \cos \theta}{n \varepsilon_{\text{bm}} L_{\text{brb}}} \quad (13)$$

Again, the displacement of the bent that corresponds to the yielding of the BRB,  $\Delta_b$ , must be smaller than the expected displacement of the bridge bent,  $\delta_e$

$$\Delta_b = \frac{n f_{yb} c_b L_{\text{brb}}}{E_s \cos \theta} < \delta_e \quad (14)$$

The total stiffness of BRBs  $K_b = K_t - K_c$ , on the basis of calculation from Step 2. The cross-sectional area of the BRB,  $A_{\text{brb}}$ , is

$$A_{\text{brb}} = \frac{\Delta_b K_b h}{4 n f_{yb} \sin \theta L_c} \quad (15)$$

where  $L_c$  = clear distance between the closely spaced CFT column in the box-pier bent case.

In both two-column bent and box-pier bent with BRBs cases, the BRB's yield strength  $F_{\text{ybrb}}$  is

$$F_{\text{ybrb}} = f_{yb} A_{\text{brb}} \quad (16)$$

After the BRB yields, strain hardening is assumed to develop in the yielding core. The largest compressive strength,  $P_{\text{ybrb}}$ , and tensile strength,  $T_{\text{ybrb}}$ , that will develop in the BRB at a given strain must be considered, particularly for capacity design purposes. Those strengths are given by

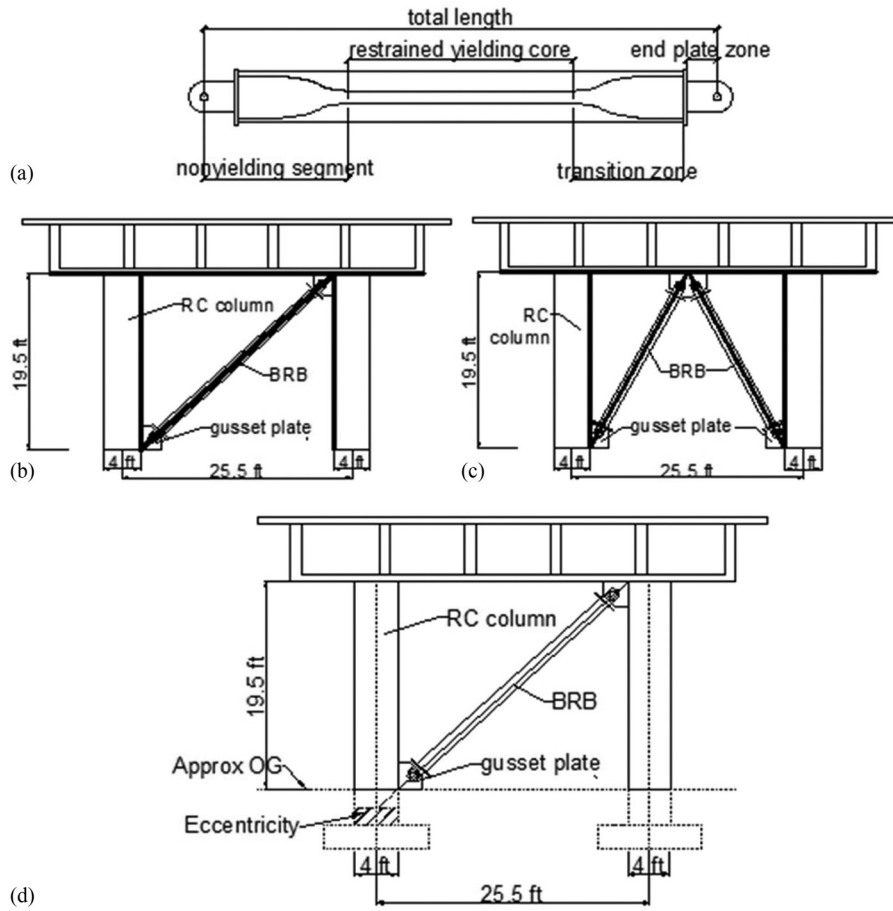


**Fig. 4.** (a) Typical steel section of a BRB; (b) transverse two-column bridge bent with BRBs, single inclined; (c) transverse two-column bridge bent with BRBs, inverted V; (d) transverse two-column bridge bent with BRBs, single inclined with eccentricity

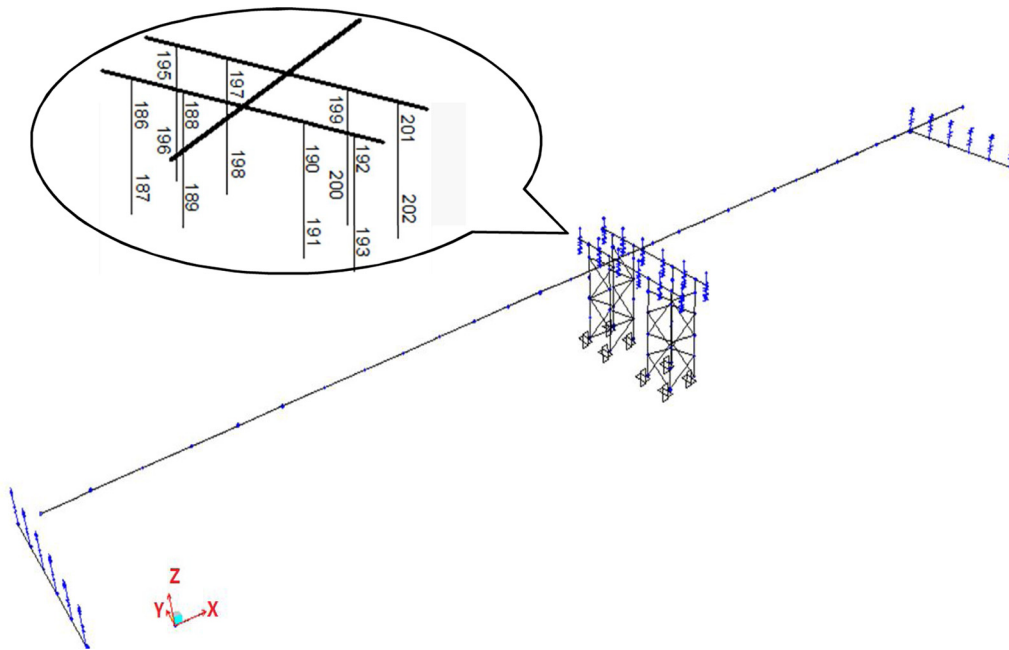


**Fig. 5.** Three-dimensional model of the bridge system with enlarged view of the bridge bents in the middle of the bridge without BRBs (with column numbering)

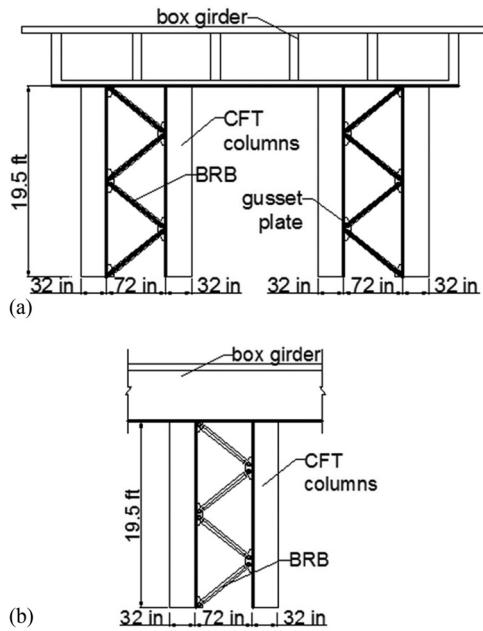


**Fig. 6.** Box pier with BRBs in the (a) transverse and (b) longitudinal directions, four BRBs between the closely spaced columns

$$P_{ybrb} = \omega \beta f_{yb} A_{brb} \quad (17)$$

$$T_{ybrb} = \omega f_{yb} A_{brb} \quad (18)$$

where  $\beta$  and  $\omega$  = strain-hardening factors, which vary with the BRB sizes and suppliers, and are assumed here to be  $\beta = 1.11$  and  $\omega = 1.35$  at 1.5% strain (López and Sabelli 2004).

#### Step 4: Column Capacity Check and Design Iteration

Once a tentative design has been reached, the column capacity at the expected displacement,  $\delta_e$ , must be checked to ensure that the column axial, flexural, and shear strength are not exceeded, considering both the seismic and service load demands (including the expected yield forces coming from BRBs per capacity design principles). Design iterations continue until a column of satisfactory strength is found.

It was observed during the process of implementing SFs in this bridge that the design of the bridge columns was governed by the seismic load cases. Therefore, results of analyses under load combinations of gravity dead and live load, and for wind loads, performed for the designs considered, are not presented here. Further detailed information can be found in Wei and Bruneau (2013).

#### Bent Pushover Analysis and Column Capacity Check

Pushover analyses of the bents was performed using the program *SAP2000* to verify development of the SF concept. To maintain the actual clear distance between the face of adjacent CFT columns to which the BRBs were added to the bent, the bridge bents were modeled by the bold lines shown in Figs. 4 and 5. The CFT columns were fixed at the top to the cap beam and at the bottom to the ground. The BRBs were pin connected to the columns. The cap beam was modeled as infinitely rigid relative to the columns by making the moment of inertia 1,000 times larger than that

corresponding to the chosen section of the cap beam. The CFT column in the analytical model was built using the *SAP2000* Section Designer. Concrete in the CFT columns had the same strength of  $2.76 \times 10^4$  kPa (4 ksi) as in the cap beam; however, the concrete in the columns was deemed to be confined. The steel shell of the CFT column was A572 Grade 60 steel. The core of the BRB was A36 steel with a yield strength of  $2.89 \times 10^5$  kPa (42 ksi), which reached  $4.34 \times 10^5$  kPa (42 ksi) and  $3.91 \times 10^5$  kPa (42 ksi) at strains of 1.5% in compression and tension, respectively.

The columns were modeled in segments, with fiber P-M<sub>2</sub>-M<sub>3</sub> hinges used at the two ends of each segment. Each fiber hinge length was 10% of the length of the member. A fiber P-M<sub>2</sub>-M<sub>3</sub> hinge was located in the middle of each BRB. However, because moments were released at the ends of the BRB (pin ends), the fiber P-M<sub>2</sub>-M<sub>3</sub> hinge, equivalent to a fiber P hinge, was used only to model the nonlinear axial behavior (resulting in trilinear behavior). Kinematic strain hardening was used in the fiber hinge of BRB. Note that Rossi (2015) compared the behavior of single-story BRB frames and analyzed it considering both isotropic and kinematic hardening, as well as smooth hysteretic curves versus bilinear curves. The differences in results obtained when using the various models were found to depend on the selected level of maximum ductility demand. On the basis of the results presented in that paper, variations in the maximum displacement demands obtained using the various hysteretic models should be no greater than 20% for the high ductility demands of the BRBs used here, given that the peak ground acceleration of the nine synthetic ground motions fell in the range of 0.7–1.0 *g*.

The dead loads, applied on the cap beam as the point load at which the webs of the box-girder are located, were used as a starting step of the nonlinear pushover analysis. The lateral load used for the pushover analysis consists of a horizontal load applied at the center of the cap beam. The horizontal displacement of the cap beam was the monitored displacement used in the displacement-control method in the pushover analysis. P-delta or second-order effect was not considered.

The elastic demand of the bridge model was obtained from a simple response spectrum analysis to assess the displacement and force demand of the bent. For consistency with results from time-history analyses presented later, the modified National Earthquake Hazards Reduction Program (NEHRP) response spectrum (BSSC 2003) in Fig. 7(a) was used. For comparison, the solid line and dotted lines correspond to, respectively, the Caltrans design acceleration spectrum specified for OSB1 and the NEHRP 2003 target design acceleration spectrum with design spectral accelerations of  $S_{D5} = 2g$ ,  $S_{D1} = 0.6g$ . The force demand of the columns in the pushover analysis was checked at the target displacement  $\delta_e$ , which is the elastic displacement demand obtained from the response spectrum analysis. The pushover curve of each analyzed bent was plotted and compared with the theoretical one developed from the SF concept. Because of the page limit, only capacity check results for the transverse bent with inverted-V BRBs and box-pier case and the pushover curve comparisons of the box pier in both directions are presented here. Additional detailed information can be found in Wei and Bruneau (2013).

#### Two-Column Bent with Inverted-V BRBs

The two-column bent with inverted-V BRB case had CFT columns of 1,219.2 mm (48 in.) in diameter with a 31.7-mm (1.25-in.)-thick steel shell. The BRBs had a cross section of  $1.1 \times 10^4$  mm<sup>2</sup> (17.178 in.<sup>2</sup>) and a yield length ratio of 0.085.

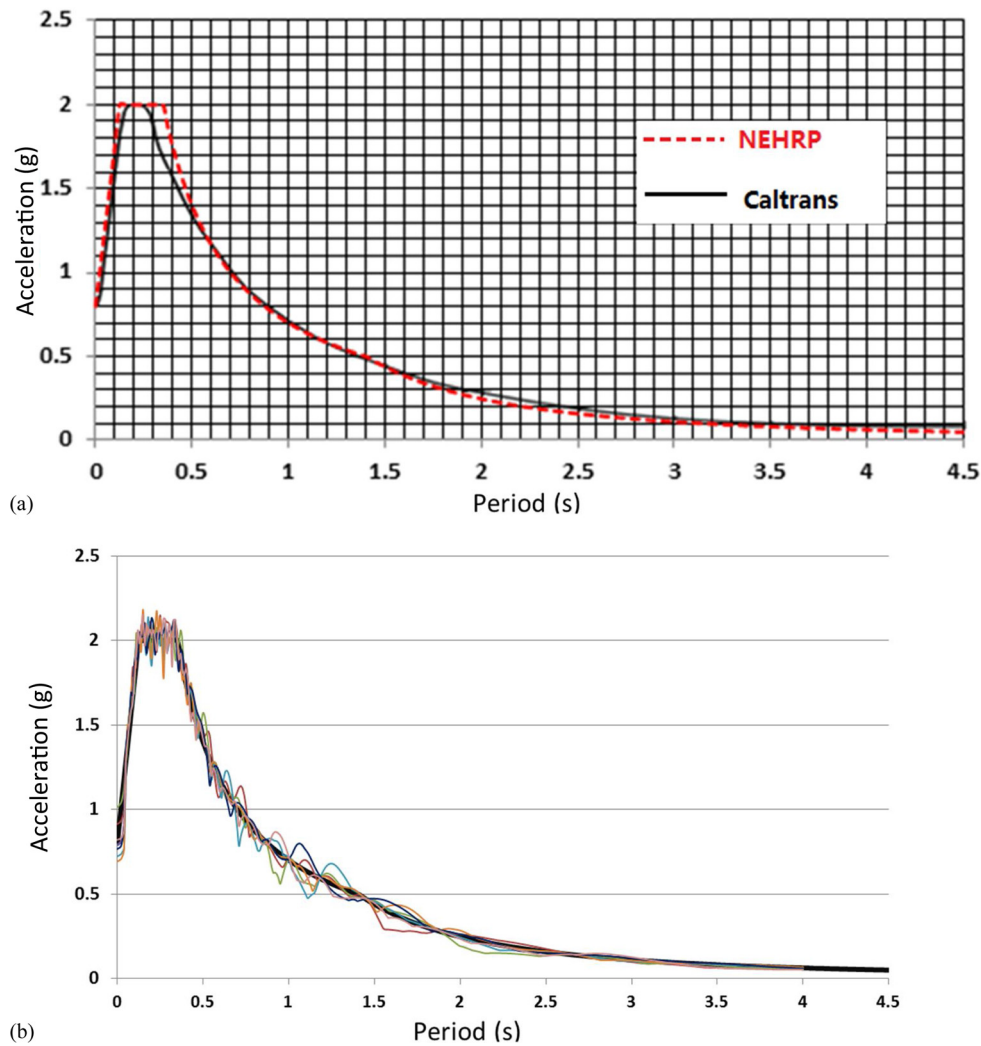


**Fig. 7.** (a) Caltrans acceleration response spectrum and corresponding NEHRP target design spectrum; (b) acceleration response spectra of the nine synthetic ground motions (damping = 5%) matching the NEHRP target design spectrum (thicker line)

The displacement demand from response spectrum analysis was 20.6 mm (0.81 in.), which is 12% larger than the column yield displacement of 18.0 mm (0.71 in.). The difference in results obtained for the design assumption and response spectrum analysis was caused by the slightly different bent stiffness considered in the *SAP2000* analyses. The designed strength and stiffness were obtained by assuming that the columns developed their yield moment,  $M_y$ , at both of their ends (assuming an infinitely rigid superstructure). The corresponding shear resistance of the frame at yield was  $2M_y/h$ , where  $h$  is the height of the column. In the *SAP2000* model, the superstructure was not as rigid as the ground, which resulted in a more flexible bent overall, and the moment at the top of the columns  $M_{top}$  was less than  $M_y$  when  $M_y$  was reached at the column bases [i.e.,  $V = (M_{top} + M_y)/h$ ]. Note that the same phenomenon was also observed in all other cases considered.

The moment and force demands at the bottom of the column were obtained from the pushover analysis when the target spectral displacement of 20.6 mm (0.81 in.) was reached, and they were compared against the provided member strengths (as shown in Table 1). Although flexural yield strength was used in the design process, a simple linear interaction equation for axial

force and plastic flexural strength was used here to check the adequacy of the column section. The flexural plastic strength and axial yield strengths listed in Table 1 are from *SAP2000* Section Designer, assuming full composite flexural strength and resistance reduction factors  $\phi$  equal to 1.0. Note that the columns were designed considering their actual slenderness, but because the resulting columns are quite stocky, slenderness had a minimal impact on their strength in this particular example. The plastic strength and axial strength interaction ratios give an indication of the columns' reserve strength. Note that the compression-flexure interaction equation given by AASHTO (2011) considers a reduction factor,  $B$ , which provides further reserve strength:

$$\frac{P_u}{P_n} + B \frac{M_u}{M_n} \leq 1 \quad (19)$$

where  $M_u/M_n \leq 1$ ;  $B = 1 - P_{rc}/P_n = 1 - \phi_c f_c A_c / P_n = 0.70$ ; and  $\phi_{c1} = 0.75$ .

The resulting ratio,  $B M_u/M_n + P_u/P_n$ , for the column in compression is 0.65, which provides a greater reserve strength. Also note that the reaction forces were used here to check the column

**Table 1.** Column Capacity Checking for Two-Column Bent with Inverted-V BRBs (With Eccentricity)

Column type	Moment demand, $M_u$ , kN-m (kPa-in)	Axial load demand, $P_u$ , kN (kPa)	Axial reaction demand, $R_u$ , kN (kPa)	Flexural strength, $\phi M_n$ , kN-m (kPa-in)	Axial strength, $\phi P_n$ , kN (kPa)	$M_u/\phi M_n + P_u/\phi P_n$
Tension	15,353 (135,884)	-1,997 (449)	1,797 (404)	20,972 (185,621)	49,019 (11,020)	<b>0.77</b>
Compression	15,080 (133,468)	-10,907 (2,452)	-15,119 (3,399)	20,972 (185,621)	-73,115 (16,437)	<b>0.93</b>

capacities, considering the eccentricity between the point at which the brace and column workline met near the foundation, as shown in Fig. 4(c). The resulting forces used were larger than those that would have been obtained otherwise, because the forces in the braces would go directly into the ground in that case (rather than in the columns first). The shear strength calculated on the basis of the equations provided by AISC (2010) and AASHTO (2014) bridge design specifications is  $1.32 \times 10^4$  kN (2,974 kips). The corresponding largest reaction shear force was  $7.29 \times 10^3$  kN (1,640 kips) (i.e., a demand-overcapacity ratio of 55%).

Although detailed results for the single-inclined BRB case are not presented here, the key findings are that the single-inclined BRB had a cross section of  $1.44 \times 10^4$  mm<sup>2</sup> (22.39 in.<sup>2</sup>) and a yield length ratio of 0.101, which is a 24% greater BRB strength than that for the inverted-V BRB case (and thus greater force demands on the connections). The structural configuration also resulted in greater demands on the columns because of the vertical component of the BRB force applied to the column by virtue of capacity design.

### Box-Pier Bent with BRBs

For the box-pier case, pushover analyses were performed for the transverse and longitudinal bents shown in Fig. 6. Note that to represent the restraint of the bent from the bridge box girder in the longitudinal direction, the cap beam was restrained to move horizontally. The resulting CFT columns were 812.8 mm (32 in.) in diameter with a steel shell 19.0 mm (0.75 in.) thick. The resulting BRBs had a yield length ratio,  $c_b$ , of 0.147 and a cross section of  $3.37 \times 10^3$  mm<sup>2</sup> (5.22 in.<sup>2</sup>). The displacement demands from the response spectrum analyses were 32.5 mm (1.28 in.) and 29.7 mm (1.17 in.) in the transverse and longitudinal directions, respectively, which are 18% and 10% larger than the column yield displacement of 26.7 mm (1.05 in.) (shown in Table 4). Smaller stiffness of the box-pier bent in the transverse and longitudinal directions were observed for the same reasons as those already presented for the two-CFT-column bent.

In an actual earthquake, seismic forces are applied simultaneously to the bent in different directions. Therefore, given that the SF concept is intended to be effective for seismic excitation in any horizontal direction, the usual 100%–30% combination of the demands in the transverse and longitudinal directions was considered here. To reflect that, this rule [expressed in terms of force combinations for elastic analyses, per Caltrans (2010) seismic design criteria (Section 2.1.2)], in fact, combines probable simultaneous displacements, as implemented later. The box-pier bents were pushed independently to the target displacements (obtained from the response spectrum analysis results) in each direction. Because the columns are considered to remain elastic, their moment demand and axial forces caused by the lateral force resisted by the bent frame was calculated on the basis of the square root of the sum of the squares of 100% of the value obtained in one direction plus 30% of the value in the other direction. Given that the BRBs already yielded at 30% of their target displacement, 100% of forces coming from the transverse and

longitudinal BRBs were applied to the columns. The corresponding forces at their strain-hardening level of 1.5% strain were added together. Note that this is somewhat conservative, because the 1.5% strain may not necessarily be reached in the direction in which 30% of the lateral load is applied. Therefore, the total controlling reaction forces at the base of the CFT columns (where the eccentricities exist) were calculated to be the maximum of the two cases: (1) 100% of longitudinal + 30% of transverse + BRB (transverse + longitudinal) + dead; and (2) 30% of longitudinal + 100% of transverse + BRB (transverse + longitudinal) + dead.

Note that forces in the columns were affected by the direction of loading (because BRBs in compression develop more force than in tension at the same drift). Therefore, two layouts were considered, namely, Layout A and Layout B for the longitudinal bent. For the frame shown in Fig. 6, Layout A corresponds to the case of a lateral load applied from left to right. For Layout B of the same frame, the load was applied from right to left. The strength of the CFT columns was checked for axial force, flexure interaction, and shear. The moment and axial load demands that resulted from the directional combination are listed in Table 2. As an example of the notation used in this table,  $L_A$  stands for longitudinal analysis for layout A. The column numbers are shown in Fig. 5(b).

The flexural plastic strength and axial yield strength, obtained from SAP2000 Section Designer fiber analysis, were checked for the axial force and moment interaction under the controlling moment and axial forces listed in Table 3. Note that the reactions were used for the axial forces, again accounting for the possibility of eccentricity. If that eccentricity did not exist, the corresponding results are shown in rows 3 and 4 in Table 3 by the no eccentricity label). The plastic moment and axial force interaction checks gave values slightly larger than 1.0 for all cases. However, it is recognized that using a linear interaction diagram is a most conservative approximation; therefore, the results were also compared with the actual interaction diagram for CFT columns in compression. The reduction factor  $B$  in Eq. (16) is 0.68. Also, the resulting ratio of  $BM_u/M_n + P_u/P_n$  for the compressive column for the case of no eccentricity would be 0.85, which makes the force and moment demands smaller than the capacity of the column.

The reaction shear forces were also calculated. Given that the column's cross section was circular, a square-root combination of the demands from the two orthogonal directions was carried out conservatively, which gave the vectorial resultant shear force acting on the columns (following the 100% and 30% combination rule for seismic forces). The shear strength calculated on the basis of the equations provided by AISC (2010) and AASHTO (2014) bridge design specifications was  $5.30 \times 10^3$  kN (1,192.5 kips). The largest shear force demands calculated from all combinations considered was  $2.88 \times 10^3$  kN (647 kips) (i.e., a demand-overcapacity ratio of 54%). Note that shear forces could reduce the column flexural strength, but there is currently no equation by AASHTO or AISC for quantifying the magnitude of this reduction for CFT columns.

Overall, the CFT columns in the box-pier case were found to have adequate strength to reach the force demands when the bridge bent reaches the target displacement (the elastic displacement demand from response spectrum analysis) for simultaneous

**Table 2.** Summarized Force Demands at the Base of the Columns

Column No.	Load combination case	Moment demand, $M_u$ , kN-m (kip-in)	Vertical reaction demand, $P_u$ , kPa (kips)
187	100% T + 30% L <sub>A</sub>	4,680 (41,425)	6,257 (1,407)
	30% T + 100% L <sub>A</sub>	4,486 (39,702)	7,282 (1,637)
	100% T + 30% L <sub>B</sub>	4,677 (41,391)	6,249 (1,405)
	30% T + 100% L <sub>B</sub>	4,441 (39,305)	7,255 (1,631)
189	100% T + 30% L <sub>A</sub>	4,971 (43,998)	-5,428 (-1,220)
	30% T + 100% L <sub>A</sub>	4,514 (39,951)	-6,095 (-1,370)
	100% T + 30% L <sub>B</sub>	4,968 (43,966)	-5,436 (-1,222)
	30% T + 100% L <sub>B</sub>	4,469 (39,556)	-6,121 (-1,376)
191	100% T + 30% L <sub>A</sub>	4,755 (42,089)	3,237 (728)
	30% T + 100% L <sub>A</sub>	4,493 (39,765)	6,376 (1,433)
	100% T + 30% L <sub>B</sub>	4,752 (42,055)	3,229 (726)
	30% T + 100% L <sub>B</sub>	4,448 (39,368)	6,349 (1,427)
193	100% T + 30% L <sub>A</sub>	4,989 (44,152)	-8,573 (-1,927)
	30% T + 100% L <sub>A</sub>	4,516 (39,966)	-7,038 (-1,582)
	100% T + 30% L <sub>B</sub>	4,985 (44,120)	-8,581 (-1,929)
	30% T + 100% L <sub>B</sub>	4,471 (39,571)	-7,065 (-1,588)
196	100% T + 30% L <sub>A</sub>	4,700 (41,599)	4,926 (1,107)
	30% T + 100% L <sub>A</sub>	4,709 (41,681)	3,465 (779)
	100% T + 30% L <sub>B</sub>	4,694 (41,547)	4,934 (1,109)
	30% T + 100% L <sub>B</sub>	4,644 (41,102)	3,492 (785)
198	100% T + 30% L <sub>A</sub>	4,990 (44,163)	-6,226 (-1,400)
	30% T + 100% L <sub>A</sub>	4,736 (41,918)	-9,377 (-2,108)
	100% T + 30% L <sub>B</sub>	4,984 (44,114)	-6,218 (-1,398)
	30% T + 100% L <sub>B</sub>	4,671 (41,343)	-9,351 (-2,102)
200	100% T + 30% L <sub>A</sub>	4,775 (42,260)	1,910 (429)
	30% T + 100% L <sub>A</sub>	4,716 (41,741)	2,564 (576)
	100% T + 30% L <sub>B</sub>	4,769 (42,209)	1,918 (431)
	30% T + 100% L <sub>B</sub>	4,651 (41,164)	2,590 (582)
202	100% T + 30% L <sub>A</sub>	5,007 (44,316)	-9,376 (-2,108)
	30% T + 100% L <sub>A</sub>	4,738 (41,932)	-10,325 (-2,321)
	100% T + 30% L <sub>B</sub>	5,002 (44,267)	-9,368 (-2,106)
	30% T + 100% L <sub>B</sub>	4,673 (41,358)	-10,299 (-2,315)

Note: T = transverse analysis for transverse bent; L<sub>A</sub> = longitudinal analysis for bent Layout A; L<sub>B</sub> = longitudinal analysis for bent Layout B.

**Table 3.** Column Capacity Checking for Box-Pier Bent (Including Case with Eccentricity)

Column type	Moment demand, $M_u$ , kN-m (kPa-in)	Reaction demand, $P_u$ , kN (kPa)	Plastic strength, $\phi M_n$ , kN-m (kPa-in)	Axial strength, $\phi P_n$ , kN (kPa)	$M_u / \phi M_n + P_u / \phi P_n$
Tension	4,680 (41,425)	6,257 (1,407)	5,614 (49,687)	19,525 (4,390)	1.15
Compression	5,001 (44,267)	-9,368 (-2,106)	5,614 (49,687)	-30,505 (-6,858)	1.20
Tension, no eccentricity	4,680 (41,425)	4,588 (1,031)	5,614 (49,687)	19,525 (4,390)	1.07
Compression, no eccentricity	4,989 (44,152)	-7,527 (-1,692)	5,614 (49,687)	-30,505 (-6,858)	1.14

earthquake demands in both the transverse and longitudinal directions.

### Box-Pier Bent Pushover Curve Comparison

The pushover curve verification was performed for the two-column bent with BRBs and box-pier bent. Only results for the transverse and longitudinal bents of the box-pier concept are discussed below. The overall comparison of the transverse pushover curve between the analysis results and the theoretical ones is shown in Fig. 8(a). The theoretical curves are indicated by dashed lines. The dashed line of the theoretical BRB shows the yielding of BRB at displacements of 2.5 mm (0.101 in.) and, at the point at which the

maximum considered strain hardening was reached, 26.7 mm (1.05 in.). The theoretical frame curve in the dashed line shows that the frame yielded at a displacement of 26.7 mm (1.05 in.), which is also the design target displacement  $\delta_e$ . The two parts add up to the total theoretical curve for the combined system plotted by the dashed line. The pushover curves obtained from SAP2000 analysis are overlaid on top of the theoretical ones as solid lines. The solid line shows the total base shear versus lateral displacement at the top of the bent. By subtracting the lateral forces resisted by the BRBs (equal to the horizontal component of the forces in the BRBs), shown by the solid line, the solid line indicates the portion of the base shear forces resisted by the bare bent alone. The target displacement demand of 32.5 mm (1.28 in.) from response spectrum analysis is indicated by the vertical line. Note

**Table 4.** Displacement of Bare Bent and Bent with BRBs for Different Systems in Theoretical Design, Response Spectrum Analysis, and Nonlinear Time-History Analysis

Case	Design target displacement			Response spectrum analysis			Nonlinear time history		
	Bare bent, mm (in.)	Bent with BRBs, mm (in.)	Difference (%)	Bare bent mm (in.)	Bent with BRBs, mm (in.)	Difference (%)	Bare bent, mm (in.)	Bent with BRBs, mm (in.)	Difference (%)
Two-CFT-column bent with single-inclined BRB	58.4 (2.30)	18.0 (0.71)	69.2	71.4 (2.81)	23.9 (0.94)	66.6	54.4 (2.14)	28.7 (1.13)	47.2
Two-CFT-column bent with inverted-V BRBs	58.4 (2.30)	18.0 (0.71)	69.2	71.4 (2.81)	20.6 (0.81)	71.2	54.4 (2.14)	27.9 (1.10)	48.8
Transverse box-pier bent	72.4 (2.85)	26.7 (1.05)	63.2	79.5 (3.13)	32.5 (1.28)	59.1	66.5 (2.62)	33.5 (1.32)	49.7
Longitudinal box-pier bent	72.4 (2.85)	26.7 (1.05)	63.2	77.7 (3.06)	29.7 (1.17)	61.8	63.8 (2.51)	32.0 (1.26)	49.7

that the theoretical bilinear curves were calculated on the basis of the flexural yield strength of the columns. The pushover curves of the bent models were obtained considering the axial force and moment interaction in the column and strain hardening in the steel tubes. Beyond the yield displacement, the pushover curves of the bent models were higher than the theoretical ones.

The overall comparison of the longitudinal bent's pushover curve between the analysis result and the theoretical ones is shown in a similar manner in Fig. 8(b), with the same solid- and dashed-line convention; the only difference is that the target elastic displacement demand from response spectrum analysis was 29.7 mm (1.17 in.) in this case.

In both cases, the pushover analysis results indicate that column yielding was first reached at the bottom of the column, where the tension and flexure interaction exists. The lower horizontal dotted line identifies the base shear resisted by the columns when that happened. The upper dotted line shows the frame shear,  $V$ , corresponding to  $2M_p/h_{\text{column}}$  calculated with  $M_p$  equal to 49,687 kip-in. (as obtained from *SAP2000* Section Designer). Note that yielding in all columns as not happening at the same time, but it occurred over small increases of frame drift. If anything, Fig. 8 shows that limiting the column demands to  $M_y$ , to prevent any column yielding, was conservative. The use of a more liberal design limit is arguably possible.

## Nonlinear Time-History Analysis

To validate the system responses previously obtained for the bridge bents using response spectrum and pushover analyses, nonlinear time-history analyses of all the previously designed bridge bents with BRBs were performed by using *SAP2000*. The nonlinear time-history analysis results enable assessment of the effectiveness of adding the SF to limit displacements by comparing them with those for the bare bridge bents without BRBs. Note that the bare bent case for the box-pier configuration is purely academic, because the box-pier system would never be used without BRBs.

The computer program Target Acceleration Spectra Compatible Time Histories (*TARSCTHS*) was used to generate nine spectrum-compatible synthetic ground motions with a time length of 25 s. That program is set up to match ground motions to the NEHRP design spectrum (BSSC 2003) as a target. In Fig. 7(b), the acceleration spectra of the nine ground motions are shown to match with the target response spectrum.

The nonlinear time-history analysis was performed for the two-dimensional (2D) bridge bent instead of the entire three-dimensional bridge, separately for the transverse and longitudinal directions. Results of the 2D bent analysis make it easier to compare with the pushover analysis results for the same bent. Out-of-plane displacements of the bent were restrained. The mass of the bridge was assigned as a linearly distributed mass on the cap beam. The self-weight of the assigned mass was not accounted for in the dead load because the mass was used only to apply the lateral seismic load to the bridge bent under the ground motions. The dead load was applied directly to the column before nonlinear time-history analysis was conducted. Hinge properties and assignments were defined the same way as was done for the pushover analyses. From the modal analysis, the mass participating ratio was more than 90% for the first two modes. Rayleigh damping was used, with coefficients corresponding to 5% damping for the first and second modal periods.

The averages of the maximum displacements in positive and negative in-plane transverse directions of the two-CFT-column bents and the box-pier bents, with and without BRBs, that resulted from the nine ground motions are shown in Table 4. The displacement histories of the bridge bents subjected to the ground motions can be found in Wei and Bruneau (2013). Results show that in all cases, displacements of the bents with BRBs had average maximum absolute lateral displacements of less than 50% of the values for cases without BRBs. Residual displacements of the bents with BRBs were generally less than 15% of the maximum displacements listed in Table 4; for comparison, this value was as high as 40% for the case without the BRBs. This result is because the columns remained predominantly elastic in the case with BRBs, thus helping provide recentering (although it was not a perfect recentering). The design displacements and the elastic displacement demands from response spectrum analyses are also shown for comparison. Note that both the design displacement and displacement demands from the response analyses of the bare bent were larger than those of the bent with BRB cases because of less lateral stiffness and a larger period.

It is shown in Table 4 that the inelastic displacement demands of the bridge bents were larger than the elastic response spectrum demand because that design was based on the *equal displacement* assumption (i.e., assuming that displacements that result from inelastic analysis are approximately equal to those obtained from a linear elastic analysis). This is usually a reasonable assumption, except for short-period structures for which it is not conservative (AASHTO 2011). Recognizing this exception, a modification factor  $R_d$  is typically prescribed to magnify the maximum elastic displacements of short-period structures and estimate the actual

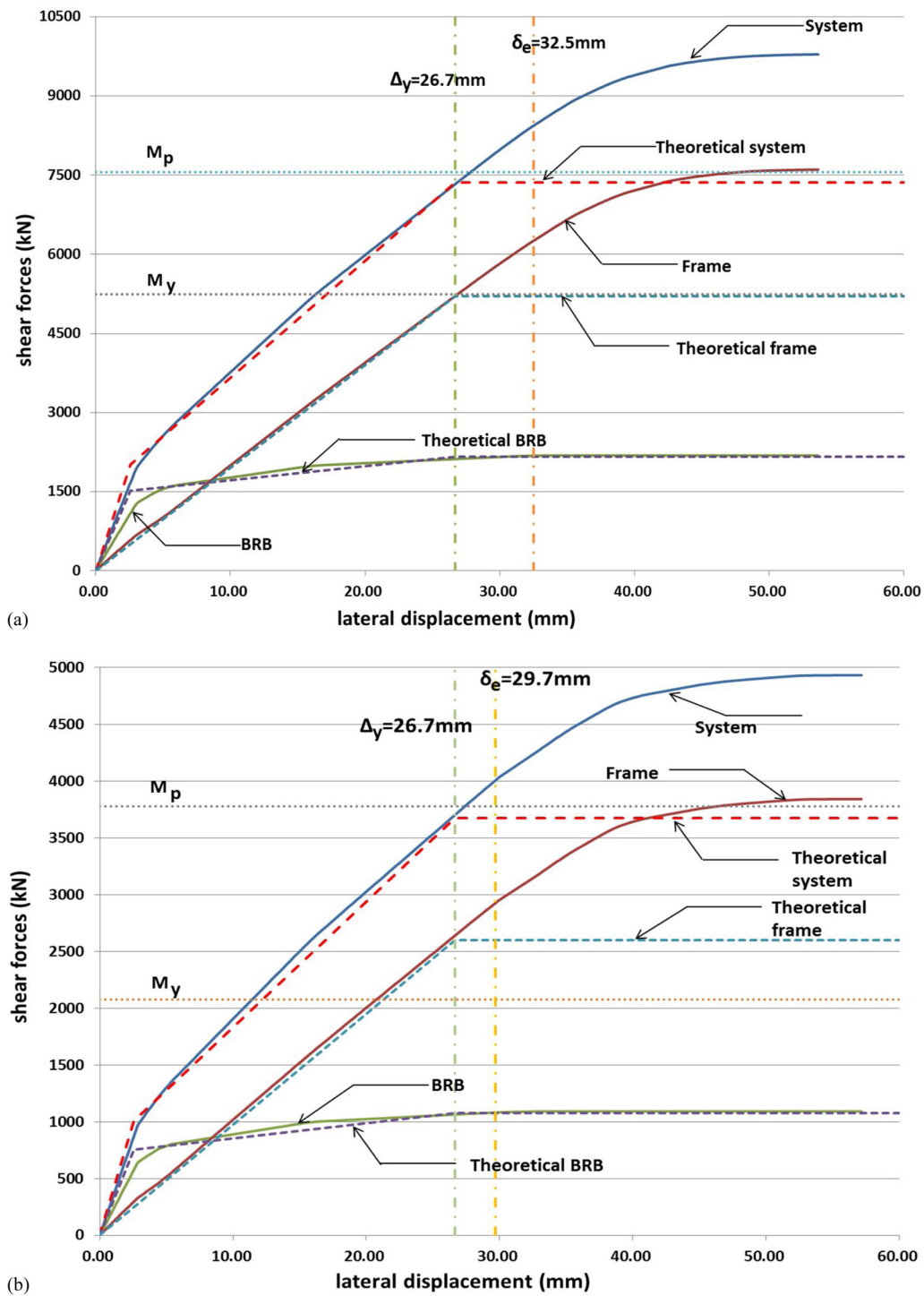


**Fig. 8.** Pushover-curve comparison between the analysis result and theoretical design value for the box pier with BRBs: (a) transverse direction; (b) longitudinal direction

maximum inelastic response, as defined by MCEER-ATC 49 (2003)

$$R_d = \frac{\Delta_{\text{inelastic}}}{\Delta_{\text{elastic}}} \quad (20)$$

When the bridge period is smaller than  $1.25T_s$ , the modification factor  $R_d$  is given by Eq. (21), from the MCEER-ATC 49 (2003) (similar to AASHTO 2011)

$$R_d = \left(1 - \frac{1}{R}\right) \frac{1.25T_s}{T} + \frac{1}{R} \geq 1 \quad (21)$$

where  $T$  = period of the bridge bent;  $T_s$  = period at the end of the acceleration response spectrum plateau; and  $R$  = ratio between design elastic lateral force and the lateral strength of the bent, which is conceptually similar to the maximum local displacement ductility demand,  $\mu_D$ , in AASHTO 2011 (conservatively, the upper limits for  $\mu_D$  according to AASHTO could have been used here instead of

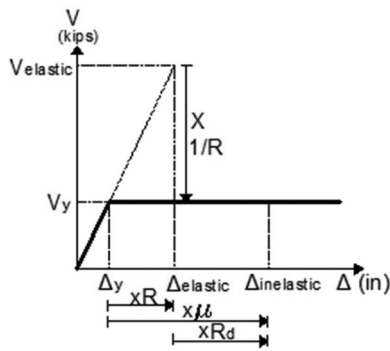


Fig. 9. Displacement modification factor for a bilinear system

Table 5. Design Displacement Amplification Factor

Bridge bent case	$R_{design}$	$R_d$ (equation)	$T_{design}$ (s)	$R_d$ (analysis)
Two-CFT-column bent with single-inclined BRB	2.92	1.85	0.19	1.47
Two-CFT-column bent with inverted-V BRBs	2.92	1.85	0.19	1.49
Transverse box-pier bent with BRBs	2.84	1.57	0.232	1.5
Longitudinal box-pier bent with BRBs	2.84	1.57	0.232	1.5

the actual value of this ratio, but it would have resulted in larger values of  $R_d$ .

The ratio  $R_{design}$  in Table 5 is the ratio between the design elastic force demand and the design lateral strength of the bent, as assumed in the design bilinear pushover curve, as shown in Fig. 9. The corresponding value  $R_d$  was calculated from Eq. (21) by using the values of  $T_{design}$  in Table 5 and 0.35 s from the acceleration response spectrum in Fig. 7(a) for T and  $T_s$ , respectively, in each bridge bent case. These actual  $R_d$  values from analyses are smaller than the value predicted by Eq. (21), which indicates that Eq. (21) is conservative for this particular application. The validation of Eq. (21) for the trilinear system, as shown in Fig. 1 for the total bent system, remains to be investigated, because it was originally developed on the basis of nonlinear time-history results of a bilinear system.

The largest base shear forces obtained from the nonlinear time-history analyses for all bent cases are compared in Table 6. The average maximum absolute base shear forces of the bridge bents with single-inclined BRBs and the inverted-V chevron BRB case are 20.7% and 20.3% higher than the no-BRB case, respectively (a relatively modest increase in base shear demands in both bridge configurations). The average maximum absolute base shear forces of the box-pier bent were 10.2% and 7.8% higher than the no-BRB case in the transverse and longitudinal directions, respectively. The design base shear forces at the design target displacement (Table 4) are also shown in Table 6. Note that no strain hardening in the columns was assumed. The base shear forces of the bent models in the pushover analyses are also tabulated in Table 6 at the spectral displacement demands from the response spectrum analyses (Table 4). The increase of the total base shear forces in the nonlinear time-history analyses from the pushover analysis was within 20% for all bents. Although shear forces in individual columns are not compared directly (for the cases before and after installation of the BRBs) in

Table 6, because the individual column's shear force was proportional to the total base shear force, the shear force demand in each column would still be within its shear capacity after adding the BRBs.

For all the bridge bent cases considered, P-M<sub>2</sub>-M<sub>3</sub> fiber hinges were located at the top and bottom of the CFT columns. The hinge behavior in the transverse and longitudinal box-pier bents, with and without BRBs, are shown and compared in Fig. 10 in terms of moment rotation history for the hinge at the bottom of the right column (which was found to develop the maximum rotation). In the transverse direction, the maximum rotation of the hinge was 0.0009 rad, which is only approximately 14% that of the no-BRB case, which had a 0.0065-rad maximum rotation. In the longitudinal direction, the maximum rotation of the hinge was 0.0017 rad, which is only approximately 20% that of the no-BRB case, which had a 0.0085-rad maximum rotation. Note that the yield rotation for the column (under its specific axial loads) was graphically estimated to be approximately 0.0006 rad. The slight amount of yielding that developed in the column is deemed acceptable for the box-pier bent with BRBs in both directions. Note that the column hinge behaviors were obtained for the bents analyzed independently for both the transverse and longitudinal directions, and the rotation could be bigger if the whole box-pier bent was applied with orthogonal ground motions simultaneously in both directions.

Figs. 11(a–d) show the hinge axial force-deformation behavior for the four BRBs located between the left two columns in the transverse box-pier model. The BRBs between the right two columns had similar behaviors. For the box-pier bent in the longitudinal direction, the axial force-deformation plots are shown in Figs. 11(e–h). In both directions, the BRBs did not yield to the same extent. The middle two BRBs developed more ductility than the top and bottom ones. Note that a compressive strength of  $1.48 \times 10^3$  kN (332 kips) and tensile strength of  $1.33 \times 10^3$  kN (299 kips) (after strain hardening) developed in the BRBs at maximum ductilities of 15 and 12.5, for the box-pier bent in the transverse and longitudinal directions, respectively.

Various possible details for connecting BRBs to other members of the bridge bent were investigated by Wei and Bruneau (2013) to establish feasibility. Welding of the BRB gusset plate to the steel shell of a CFT emerged as the preferred approach among those considered, particularly for large BRBs, but alternative details are also possible. Design of BRBs to the cap beam and foundation using anchor bolts or anchor rods were also investigated and found to be practical only for small BRBs.

## Conclusions

The results presented in this case study demonstrate that bridge bents using BRBs as SFs can be designed and can be effective in improving seismic behavior. A conservative design objective of full elastic column response was considered in this study by limiting demands in the columns to their yield flexural strength ( $M_y$ ). Although this made design of the SFs more challenging, it remained possible to implement such fuses in the bridge bent to resist earthquake excitations from the transverse direction or from two orthogonal directions.

The columns had sufficient strength to resist the force demand (considering axial and flexural interaction) at the target displacement in the pushover analyses. A comparison of theoretical and actual pushover curves in both the two-CFT-column and box-pier-column cases showed good results, which indicates that bridge bent behavior was consistent with that predicted by the SF concept.

**Table 6.** Base Shear Force of Bare Bent and Bent with BRBs for Different Systems in Theoretical Design Calculation, Pushover Analyses, and Nonlinear Time-history Analysis

Case	Design calculation			Pushover			Nonlinear time history		
	Bare bent, kN (kips)	Bent with BRBs, kN (kips)	Difference (%)	Bare bent, kN (kips)	Bent with BRBs, kN (kips)	Difference (%)	Bare bent, kN (kips)	Bent with BRBs, kN (kips)	Difference (%)
Two-CFT-column bent with single-inclined BRB	9,648 (2,169)	13,318 (2,994)	38	14,136 (3,178)	16,014 (3,600)	13.3	14,439 (3,246)	17,424 (3,917)	20.7
Two-CFT-column bent with inverted-V BRBs	9,648 (2,169)	13,296 (2,989)	38	14,123 (3,175)	14,492 (3,258)	2.6	14,439 (3,246)	17,370 (3,905)	20.3
Transverse box-pier bent	5,200 (1,169)	7,357 (1,654)	41	7,602 (1,709)	8,438 (1,897)	11	7,789 (1,751)	8,585 (1,930)	10.2
Longitudinal box-pier bent	2,602 (585)	3,679 (827)	41	3,843 (864)	4,012 (902)	4.4	3,923 (882)	4,230 (951)	7.8

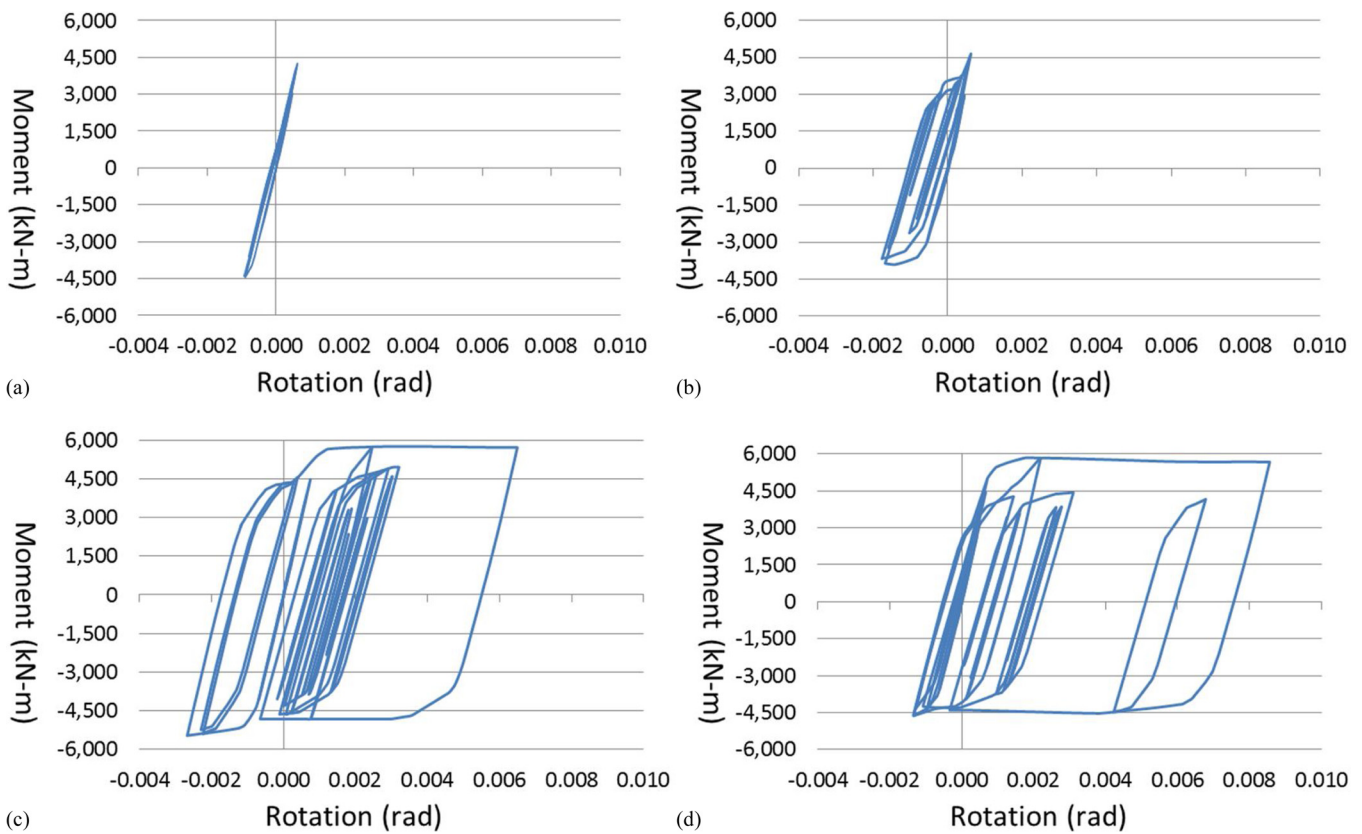


**Fig. 10.** Hinge behaviors at bottom of the rightmost column of the box-pier bent (a) transverse with BRB, (b) longitudinal with BRB, (c) transverse no BRB, and (d) longitudinal no BRB

Nonlinear time-history analysis was also performed to verify the behavior of the bridge bents compared to the responses predicted by the design procedure, elastic response spectrum, and pushover analysis. Displacement at the bent cap beam level and base shear force demand were compared for the bridge bents with BRBs in each case with their corresponding bare bent. For all the bents designed with BRBs, drift reductions of at least 50% were accompanied by modest increases in base shear demands no greater than 20%. The inelastic displacement demands of the bridge bent model were found to slightly exceed predictions based on the elastic displacements from the response spectrum analyses, which was a consequence of using a constant strength-reduction factor as part of the design procedure (which is known to result in greater inelastic displacement for structures that have short periods).

Although this case study shows concept feasibility, much research is needed to optimize SF design parameters, enhance accuracy of response predictions, and establish bounds within which effective solutions are possible.

### Acknowledgments

This study was sponsored by Caltrans under research Contract Number 65A0432. The authors acknowledge the valuable comments and feedback from Caltrans. However, any opinions, findings, conclusions, and recommendations presented in this report are those of the writers and do not necessarily reflect the views of the sponsor.

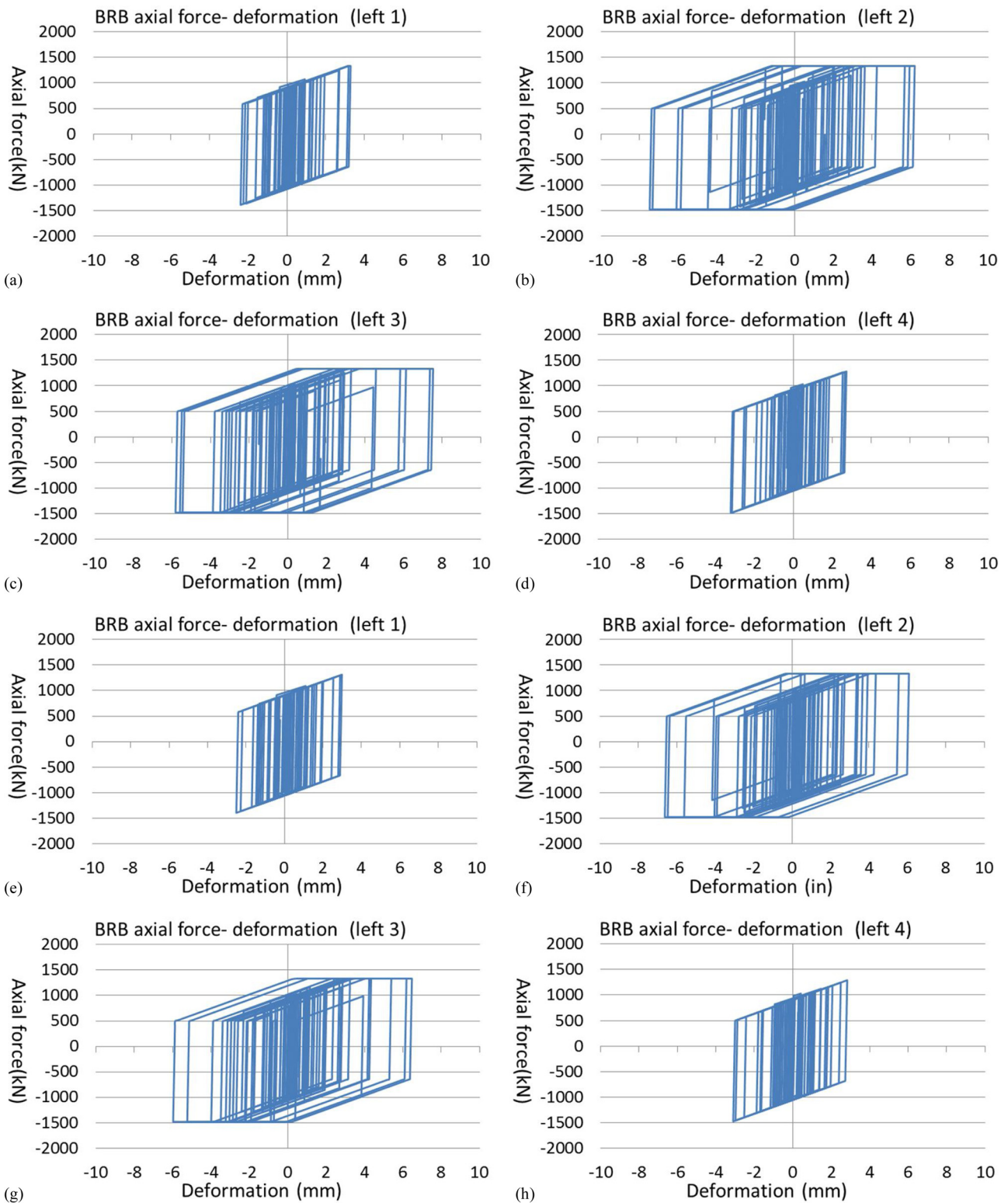


**Fig. 11.** BRB hinge axial force-deformation plot for the box-pier bridge bent: (a–d) for the four BRBs located between the left two columns in the transverse bent ; (e–h) for the four BRBs located between the two columns in the longitudinal bent (numbered from 1 to 4 for BRBs from top to bottom)

## References

AASHTO. (2011). "AASHTO guide specifications for LRFD seismic bridge design." 2nd Ed. Washington, DC.  
 AASHTO. (2014). "AASHTO LRFD bridge design specifications." 7th Ed. Washington, DC.

Aiken, I. D., Clark, P. W., Tajirian, F. F., Kasai, K., Kimura, I., and Ko, E. (2000). "Unbonded braces in the United States—Design studies, large-scale testing and the first building application." *Proc., Japan Passive Control Symp.*, Tokyo Institute of Technology, Japan.  
 AISC. (2010). "Seismic provisions for structural steel buildings." *AISC 341-10*, Chicago.

- BSSC (Building Seismic Safety Council). (2003). *NEHRP recommended provisions and commentary for seismic regulations for new buildings and other structures (FEMA 450)*, Washington, DC.
- Caltrans (California Department of Transportation). (2010). "Caltrans seismic design criteria." Version 1.6, Sacramento, CA.
- Carden, L., Itani, A. P. E., and Buckle, F. I. (2006). "Seismic performance of steel girder bridges with ductile cross frames using buckling-restrained braces." *J. Struct. Eng.*, **10.1061/(ASCE)0733-9445(2006)132:3(338)**, 338–345.
- Clark, P., Aiken, I., Kasai, K., and Kimura, I. (2000). "Large-scale testing of steel unbonded braces for energy dissipation." *Adv. Technol. Struct. Eng.*, **1–5**.
- El-Bahey, S., and Bruneau, M. (2010). "Analytical development and experimental validation of a structural-fuse bridge pier concept." *Tech. Rep. MCEER-10-0005*, MCEER, Univ. at Buffalo, Buffalo, NY.
- Hamada, N., Nishioka, T., and Kanaji, H. (2007). "Seismic retrofitting of long-span truss bridge-Minato Bridge using damage-control technologies." *Steel Constr. Today Tomorrow*, **19**, 12–16.
- Kanaji, H., Kitazawa, M., and Suzuki, N. (2005). "Seismic retrofit strategy using damage control design concept and the response reduction effect for a long-span truss bridge." *Proc., 19th US-Japan Bridge Eng. Workshop: UJNR Panel on Wind and Seismic Effects*, United States/ Japan Natural Resources Development Program, Tsukuba, Japan.
- Lanning, J., Benzoni, G., and Uang, C. M. (2011). "The feasibility of using buckling-restrained braces for long-span bridges, a case study." *Tech. Rep. CA12-2149*, Caltrans, Sacramento, CA.
- Lopez, W., Gwie, D., Saunders, M., and Lauck, T. (2002). "Lessons learned from large-scale tests of unbonded braced frame subassembly." *Proc., 71st Annual Convention*, Structural Engineers Association of California, Sacramento, CA, 171–183.
- López, W. A., and Sabelli, R. (2004). "Steel tips report: Seismic design of buckling-restrained braced frames." Structural Steel Educational Council, Lafayette, CA.
- MCEER-ATC 49 (2003). "Recommended LRFD guidelines for the seismic design of highway bridges." *Tech. Rep. MCEER-03-SP03*, MCEER, Univ. at Buffalo, Buffalo, NY.
- Oya, T., Fukasawa, T., Fujiwara, M., et al. (2009). "Practical study on a new type buckling-retrained-brace." *Proc., Int. Association for Shell and Spatial Structure (IASS) Symp.*, Editorial Universitat Politècnica de València, València, Spain.
- Reno, M. L., and Pohl, M. N. (2010). "Seismic retrofit of California's Auburn-Foresthill Bridge." *Transportation Research Record*, **2201/2010**, 83–94.
- Rossi, P. (2015). "Importance of isotropic hardening in the modeling of buckling restrained braces." *J. Struct. Eng.*, **10.1061/(ASCE)ST.1943-541X.0001031**, 04014124.
- SAP2000 14 [Computer software]. Computers & Structures, Inc., Walnut Creek, CA.
- TARSCTHS (Target Acceleration Spectra Compatible Time Histories) [Computer software]. Version 1, Univ. at Buffalo, Buffalo, NY.
- Uang, C. M., Bruneau, M. K., and Tsai, C. (2014). "Seismic design of steel bridges" *The CRC handbook of bridge engineering—Seismic design*, CRC Press, Boca Raton, FL, 301–336.
- Usami, T., Lu, Z., and Ge, H. (2005). "A seismic upgrading method for steel arch bridges using buckling-restrained braces." *Earthquake Eng. Struct. Dyn.*, **34(4–5)**, 471–496.
- Vargas, R., and Bruneau, M. (2006). "Experimental investigation of the structural fuse concept." *Tech. Rep. MCEER-06-0005*, MCEER, Univ. at Buffalo, Buffalo, NY.
- Wada, A., Huang, Y. H., and Iwata, M. (2000). "Passive damping technology for buildings in Japan." *Prog. Struct. Mater. Eng.*, **2(3)**, 335–350.
- Wei, X., and Bruneau, M. (2013). "Resilient bridges: Replaceable structural fuses for post-earthquake accelerated service, phase 1: Analytical investigation." *Tech. Rep. CA13-2296*, Caltrans, Sacramento, CA.
- Zahrai, S. M., and Bruneau, M. (1999). "Ductile end-diaphragms for seismic retrofit of slab-on-girder steel bridges." *J. Struct. Eng.*, **10.1061/(ASCE)0733-9445(1999)125:1(71)**, 71–80.